Adsorption (2013) 19:945–957
DOI 10.1007/s10450-013-9502-y

Role of pore volume and surface diffusion in the adsorption of aromatic compounds on activated carbon

R. Ocampo-Pérez · R. Leyva-Ramos · M. Sanchez-Polo · J. Rivera-Utrilla

Received: 14 February 2012 / Accepted: 4 February 2013 / Published online: 20 February 2013
© Springer Science+Business Media New York 2013

Abstract The objective of this manuscript was to elucidate the main mechanism of mass transport involved in intraparticle diffusion during the adsorption of phenol, methylene blue (MB), and methyl blue (MTB) on granular activated carbon (AC F400) by using three diffusional models: (i) pore volume diffusion model (PVDM), (ii) pore volume and surface diffusion model (PVSDM), and (iii) surface diffusion model (SDM). Results revealed that the molecular size of the organic compounds as well as its adsorption capacity considerably affect their overall adsorption rate as well as controlling the mass transfer mechanism. The PVSDM model, which assumes that pore volume and surface diffusion are both important in intraparticle diffusion, satisfactorily fitted the experimental data. The percentage contribution of surface diffusion to overall intraparticle diffusion was >82 % for phenol, 19 % for MTB and 5–95 % for MB. These results confirmed that the controlling mechanism of the overall adsorption rate on AC F400 is surface diffusion for phenol and pore volume diffusion for MTB, while both diffusion mechanisms are important in the adsorption of MB. The SDM modeled reasonably well the concentration decay data for phenol adsorption under different experimental conditions. Furthermore, it was found that surface diffusion coefficient values augmented as the amount of phenol adsorbed at equilibrium increased. The PVDM model fitted the experimental MTB decay data reasonably well, showing that the tortuosity factor of AC F400 ranged from 3 to 5. The external mass transport did not affect the overall rate of phenol, MB and MTB adsorption on AC F400.

Keywords Activated carbon · Adsorption rate · Diffusional models · Aromatic compounds

Abbreviations

a	Prausnitz–Radke isotherm constant (L/g)
b	Prausnitz–Radke isotherm constant ($mmol^{-\beta}L^{\beta}$)
C_A	Concentration of adsorbate in aqueous solution (mmol/L)
C_{A0}	Initial concentration of adsorbate in aqueous solution (mmol/L)
C_{Ar}	Concentration of adsorbate within the particle at distance r (mmol/L)
$C_{Ar\|r=Rp}$	Concentration of adsorbate at the external surface of the particle at $r = R_p$ (mmol/L)
d_p	Average pore diameter (nm)
D_{AB}	Molecular diffusion coefficient at infinite dilution (cm^2/s)
D_{ep}	Effective pore volume diffusion coefficient (cm^2/s)
D_s	Surface diffusion coefficient (cm^2/s)
k_L	External mass transfer coefficient in liquid phase (cm/s)
m	Mass of adsorbent (g)
q_e	Amount of adsorbate adsorbed at equilibrium (mmol/g)
q_{exp}	Experimental amount of solute adsorbed (mmol/g)
q_{pred}	Amount of solute adsorbed predicted with the isotherm model (mmol/g)

R. Ocampo-Pérez · M. Sanchez-Polo · J. Rivera-Utrilla
Departamento de Quimica Inorganica, Facultad de Ciencias, Universidad de Granada, 18071 Granada, Spain

R. Ocampo-Pérez (✉) · R. Leyva-Ramos
Facultad de Ciencias Quimicas, Centro de Investigacion y Estudios de Posgrado, Universidad Autonoma de San Luis Potosi, Av. Dr. M. Nava No. 6, 78210 San Luis Potosi, SLP, Mexico
e-mail: raul_iqi@yahoo.com.mx

r	Radial distance (cm)
R_p	Radius of the particle (cm)
S	External surface area per mass of adsorbent (cm^2/g)
V	Volume of the solution (mL)
β	Prausnitz–Radke isotherm constant
ε_p	Void fraction of AC F400 particles
ρ_p	Density of adsorbent particles (g/mL)
τ	Tortuosity factor
ϕ_A	Dimensionless concentration of adsorbate in the solution
ϕ_{exp}	Experimental dimensionless concentration of adsorbate in the solution
ϕ_{pred}	Dimensionless concentration of adsorbate in the solution predicted with the diffusional models

1 Introduction

Aromatic organic compounds such as phenolic compounds and dyes are important materials in the chemical industry. They are used as raw materials in numerous chemical productions and often employed in the manufacture of plastics, pigments, paints, and paper. Because these organic compounds have been classified as toxic, carcinogenic, and/or mutagenic agents, their presence in water stream even at low concentrations is of major environmental concern (Wibowo et al. 2007). Dyes generally consist of complex aromatic compounds that provide stability against biodegradation in aquatic ecosystems (Verma 2011). Therefore, removal of phenolic compounds and dyes from the effluents of industries is of paramount importance to maintain the health of the ecosystem.

Activated carbon (AC) is one of the most important microporous adsorbents from an industrial standpoint. It has highly complex surface characteristics (porosity and surface chemistry), with pore sizes that range from micropores (<2 nm) to macropores (>50 nm) and a variety of surface groups (Rivera-Utrilla et al. 2011). AC F400 is a typical granular activated carbon (GAC) manufactured from a bituminous carbon by Calgon Carbon Corporation. It has been widely used for the removal of dyes (Yang and Al-Duri 2005), aromatic compounds (Wibowo et al. 2007), heavy metals (Mohan et al. 2007), oxyanions (Mahmudov and Huang 2011), volatile organic compounds (Chiang et al. 2001), and surfactants (Fulazzaky 2011). The capacity of AC F400 to adsorb phenol and dyes has been investigated by various authors. Cañizares et al. (2006) studied the adsorption of phenol solutions onto AC F400 and AC F400 modified with 2 N hydrochloric acid. They found that the acid treatment had no significant effect on the surface area of the AC F400 and that the adsorption equilibrium decreased with higher temperature, indicating exothermic adsorption. The adsorption capacity was maximal at pH 3 and 7 and lower at pH 13. The removal of methylene blue (MB) by adsorption onto AC F400 was investigated by El Qada et al. (2008), who found that the pH had a small effect on the adsorption capacity, which rose from 430 to 476 mg/g when the pH was increased from 4 to 11; they also reported that the adsorption capacity was not enhanced by a reduction in particle size.

The design of an adsorption system requires data on the concentration decay curves of the adsorbate/adsorbent system and on the adsorption capacity of the adsorbent as a function of adsorbate concentration (adsorption isotherm). The estimation of adsorption kinetic parameters involves comparing experimental concentration decay curves with those predicted by a model, which can have an empirical or theoretical basis. Several models can be utilized, depending on whether the transport mechanism within the particle is assumed to be diffusion in liquid-filled pores, diffusion in adsorbed phase (surface diffusion), or both mechanisms in parallel (Sotelo et al. 2002).

The surface diffusional model (SDM) is the most widely used model to interpret concentration decay curves of aromatic compounds on AC F400; it assumes that the intraparticle diffusion is exclusively due to surface diffusion and that there is no pore volume diffusion. The SDM model has been utilized to fit the kinetic data of 2,4-dichlorophenoxyacetic acid, dyes, *p*-chlorophenol, 2-nitrophenol and pyridine, obtaining a surface diffusion coefficient (D_s) of 1.90×10^{-9}, 2.3×10^{-10}–2.00×10^{-11}, 1.90×10^{-8}, 1.08×10^{-7}, and 2×10^{-7} cm^2/s, respectively (Ocampo-Perez et al. 2010; Al Duri and Mckay 1988; Sze and McKay 2012; Karimi-Jashni and Narbaitz 1997; Kim et al. 2002). These results indicate that the value of D_s depends on the adsorbate molecular size. D_s was also found to depend on the temperature and the mass adsorbed at equilibrium.

With this background, the main aim of this study was to elucidate the mechanism of mass transport involved in the intraparticle diffusion of phenol, MB, and methyl blue (MTB) on AC F400 by using three diffusional models, (i) pore volume diffusion model (PVDM), (ii) pore volume and surface diffusion model (PVSDM), and (iii) surface diffusion model (SDM). Moreover, the relationship between the molecular size of the adsorbates and the adsorption diffusion mechanism is also investigated.

2 Materials and methods

2.1 Adsorbent

The GAC used in this study was manufactured from a bituminous carbon by Calgon Inc. (Pittsburgh, PA) and is

commercially available as F400. The AC F400 was sieved to three portions of average particle radius of 0.050, 0.010 and 0.005 cm, washed several times with deionized water, dried in an oven at 110 °C for 24 h, and stored in a plastic container.

Textural characterization was carried out by gas adsorption (N_2 at 77 °C and CO_2 at 273 K) using an Autosorb 1 from Quantachrome after outgassing the samples overnight at 110 °C under high vacuum (10^{-6} mbar). The pressure range used was $1 \times 10^{-6} < P/P_0 < 1$ The BET and Dubinin–Radushkevich equations were applied to determine the apparent surface area (S_{BET}) and micropore volume (W_0), respectively. In the absence of restrictions, $W_0(N_2)$ yields the total micropore volume while $W_0(CO_2)$ estimates the narrowest microporosity (micropores <0.7 nm in diameter) (Gil and Grange 1996). The mean micropore width (L_0) and micropore surface area (S_{CO2}) were estimated by applying the Stoeckli equation to the CO_2 adsorption data and the pore size distribution (PSD) was determined by applying quenched solid density functional theory (QSDFT) to the N_2 adsorption isotherms, assuming slit-shaped pores. The density of the solid was determined by the Helium displacement method using a Micromeritics Accupic 1330 helium pycnometer.

Total surface acidity and basicity were determined by titration with NaOH and HCl, respectively, following a previously described method (Diaz-Flores et al. 2006). The pH of the point of zero charge (pH_{pzc}) was obtained by preparing 25 mL of 0.01 N NaCl solutions with different initial pH values, adding different volumes of 0.01 N NaOH and HCl for this purpose. Nitrogen was bubbled through the solutions to avoid CO_2 dissolution, followed by the addition of 50 mg of the activated carbon. Activated carbon and solutions were left in contact for 48 h, and the final solution pH was then measured. The initial pH was plotted against the final solution pH, and the point at which the lines crossed was considered the pH_{pzc}.

2.2 Adsorbates

All adsorbates used in this study were reagent grade. Phenol was supplied by Fermont and MB and MTB by Sigma-Aldrich. The molecular structure and physical properties of these adsorbates are exhibited in Table 1. According to their pKa values and the working pH (3), phenol molecules will be in molecular form, while MB and MTB molecules will be in cationic and anionic form, respectively. The molecular structures of these organic compounds were calculated by using Chem3D Ultra 9.0 software.

2.3 Determination of adsorbate concentration in water solution

The phenol, MB, or MTB concentration in an aqueous solution was determined by UV–Vis spectroscopy using a Shimadzu UV-160 spectrophotometer at wavelengths of 269.5, 665, and 598 nm, respectively.

2.4 Adsorption equilibrium data

A batch adsorber consisting of a 50 mL plastic centrifuge vial was used to obtain the adsorption equilibrium data for each compound on AC F400. For this purpose, 0.1 g of carbon and 40 mL of an adsorbate solution with a known initial concentration (range, 0.1–4 mmol/L) were added to the batch adsorber, which was partially immersed in a water bath at constant temperature. The solution and carbon particles remained in contact until equilibrium was reached. Preliminary experiments indicated that intervals

Table 1 Physicochemical properties of adsorbates

Adsorbate	Molecular structure	Molecular formula	pK_a	MW (g/mol)	Dimensions X, Y, Z (nm)
Phenol	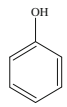	C_6H_6O	9.86	94.11	0.675 0.706 0.296
MB	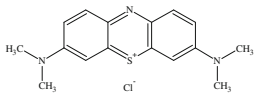	$C_{16}H_{18}N_3SCl$	3.80	319.85	1.641 0.744 0.617
MTB	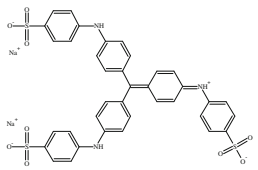	$C_{37}H_{27}N_3Na_2O_9S_3$	8.80	799.81	2.1 1.36 0.81

of 1, 2, and 3 days were sufficient to attain equilibrium of phenol, MB, and MTB, respectively. The solution pH was measured periodically and maintained constant by adding 0.01 N of HCl and NaOH solutions as needed. Once equilibrium was reached, the final concentration of adsorbate was determined and the mass of solute adsorbed was estimated by means of the following equation:

$$q = \frac{V(C_{A0} - C_{Ae})}{m} \tag{1}$$

2.5 Method for obtaining adsorption rate data

The experimental concentration decay curves for the three organic compounds were obtained in a batch stirred tank adsorber. This adsorber was a 500 mL acrylic container with a funnel-shaped base to which a cellulose acetate membrane was clamped. The membrane had a diameter of 4.5 cm and pore opening of 0.2 μm. The temperature of the solution in the adsorber was kept constant by circulating water through a glass coil immersed in the solution. The solution and carbon were continuously mixed with a propeller agitator attached to a variable-speed motor. The adsorber solution was sampled by applying a vacuum and filtering the solution through the membrane at the bottom of the adsorber.

Concentration decay data for adsorption of phenol, MB, and MTB on AC F400 were obtained by the following procedure. A solution was prepared in a 500 mL volumetric flask at pH 3 by mixing appropriate volumes of 0.01 N of HCl and NaOH. An aliquot of a given volume was removed and the remaining solution was added to the adsorber, which contained 0.5–3 g of AC F400. The agitation speed was set up at 400 rpm. The solution pH was periodically measured and maintained at pH 3 by adding 0.01 N HCl and NaOH solutions as required. The solution and the GAC were left in contact until the temperature and pH remained constant over time. Then, a known concentration of the adsorbate solution was rapidly added to the adsorber solution and the timer and stirrer motor were activated. The temperature and pH of the solution were periodically measured and the solution pH was kept constant as described above. The adsorber solution was periodically sampled by removing 1 mL and determining the concentration of the sample.

The dimensionless adsorbate concentration was calculated with the following equation:

$$\phi_A = \frac{C_A}{C_{A0}} \tag{2}$$

The dimensionless phenol, MB, or MTB concentration was plotted against time to obtain the dimensionless concentration decay curve.

3 Diffusional models

The concentration decay curves of phenol, MB and MTB were modeled by using three diffusional models derived by assuming the following: (i) intraparticle diffusion occurs by pore volume diffusion (Fick diffusion) and surface diffusion, (ii) the rate of adsorption on an active site is instantaneous, and (iii) carbon particles are spherical. Model equations and initial and boundary conditions are (Leyva-Ramos and Geankoplis 1994):

$$V\frac{dC_A}{dt} = -mSk_L\left(C_A - C_{Ar}|_{r=R_p}\right) \tag{3}$$

$$t = 0 \quad C_A = C_{A0} \tag{4}$$

$$\varepsilon_p\frac{\partial C_{Ar}}{\partial t} + \rho_p\frac{\partial q}{\partial t} = \frac{1}{r^2}\frac{\partial}{\partial r}\left[r^2\left(D_{ep}\frac{\partial C_{Ar}}{\partial r} + D_s\rho_p\frac{\partial q}{\partial r}\right)\right] \tag{5}$$

$$C_{Ar} = 0 \quad t = 0 \quad 0 \le r \le R_p \tag{6}$$

$$\left.\frac{\partial C_{Ar}}{\partial t}\right|_{r=0} = 0 \tag{7}$$

$$D_{ep}\left.\frac{\partial C_{Ar}}{\partial r}\right|_{r=R} + D_s\rho_p\frac{\partial q}{\partial r} = k_L\left(C_A - C_{Ar}|_{r=R_p}\right) \tag{8}$$

The model represented by Eqs. (3)–(8) is the general diffusional model (PVSDM). The parameters k_L, D_s, and D_{ep} correspond to external transport, surface diffusion, and pore volume diffusion mechanisms, respectively. The general model can be simplified by considering that the sole intraparticle diffusion mechanism may be either pore volume diffusion (PVDM) ($D_{ep} \neq 0$, $D_s = 0$) or surface diffusion (SDM) ($D_{ep} = 0$, $D_s \neq 0$).

4 Results and discussion

4.1 Characterization of AC F400

Figure 1 depicts the N_2 adsorption/desorption isotherm at 77 K, showing a type I profile characteristic of microporous materials (BET classification) and a type H4 hysteresis loop characteristic of narrow slit-like pores. This figure also contains the PSD estimated by QSDFT, evidencing a large proportion of micropores with a pore width of 0.9 nm.

Table 2 lists the chemical and textural properties of AC F400. It showed a high apparent specific surface area ($S_{BET} = 877$ m^2/g) and consisted largely of narrow micropores ($S_{mic} = 706$ m^2/g) with a mean size (L_0) of 0.73 nm. It had a slightly basic character ($pH_{PZC} = 7.5$). The density (ρ_s) of AC F400 was 2.32 g/cm^3; the particle density (ρ_p) 1.036 g/cm^3, and the void fraction (ε_p) 0.554.

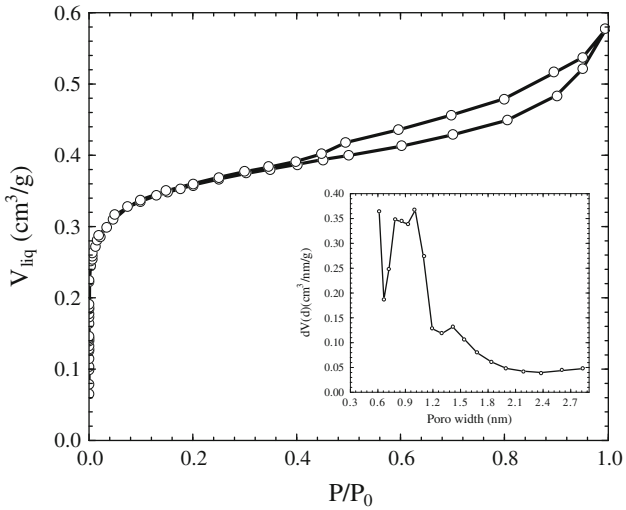

Fig. 1 Nitrogen adsorption isotherm and pore size distribution of AC F400 at 77 K

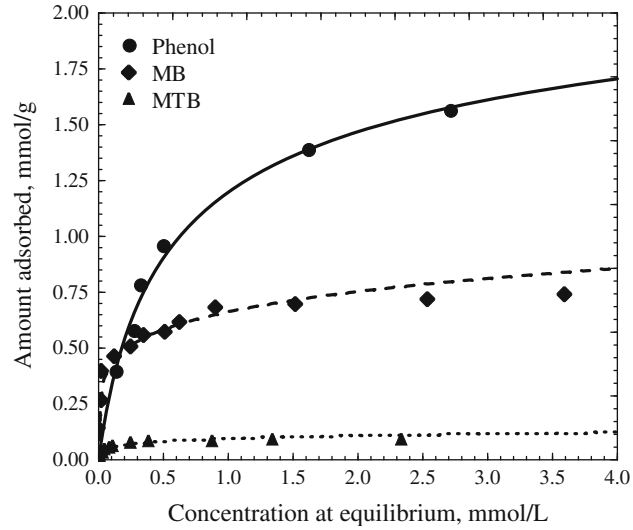

Fig. 2 Adsorption isotherms of phenol, MB, and MTB on AC F400 at pH 3 and T = 298 K. *Lines* represent Prausnitz–Radke isotherms

4.2 Adsorption isotherm of the organic compounds

Figure 2 shows the adsorption equilibrium of phenol, MB and MTB on AC F400 at pH 3 and T 298 K, clearly showing that AC F400 had the highest adsorption capacity to adsorb phenol, followed by MB and MTB. Thus, at an equilibrium concentration of 2.5 mmol/L, an adsorption capacity of 1.56, 0.75, and 0.12 mmol/L was found for phenol, MB, and MTB, respectively. Hence, the capacity of AC F400 to adsorb phenol was 2- and 13-fold higher than its capacity to adsorb MB and MTB, respectively. These results can be explained by the fact that only the phenol molecule can diffuse through the narrow microporosity of AC F400 ($L_0 = 0.73$ nm) and therefore adsorb on almost all of the exposed surface area. In contrast, the MB molecule (depending on its orientation) can be adsorbed on the surface area formed by pores larger than 0.75 nm, which represent only 26 % of the total pore volume. Finally, for reasons of molecular size and hindered factors, MTB can only be adsorbed on the surface corresponding to the meso- and macroporosity of AC F400, which is why it was the least adsorbed compound on this highly microporous material.

The experimental adsorption equilibrium data of phenol, MB, and MTB were interpreted by using the Prausnitz–Radke adsorption isotherm model, which can be represented by the following equation:

$$q = \frac{aC}{1 + bC^{\beta}} \tag{9}$$

The adsorption constants were calculated by means of a non-linear estimation method using Statistica software. Table 3 gives the isotherm constant values and mean absolute percentage deviations. Percentage deviations were calculated with the following equation:

$$\%D = \frac{1}{N}\sum_{i=1}^{N}\left|\frac{q_{exp} - q_{pred}}{q_{exp}}\right| \times 100\% \tag{10}$$

Prausnitz–Radke isotherm and adsorption equilibrium data are depicted in Fig. 2. Percentage deviations were <5 %, indicating that the Prausnitz–Radke model fitted to the adsorption equilibrium data reasonably well.

4.3 Experimental concentration decay curves of phenol, MB, and MTB

During the adsorption rate experiments, a continuous increase in the solution pH was observed. If the solution pH were not kept constant, the adsorption equilibrium would

Table 2 Textural and chemical characteristics of AC F400

Sample	N_2				CO_2				Total acid groups (meq/g)	Total basic groups (meq/g)	pH_{PZC}
	S_{BET} (m^2/g)	W_0 (cm^3/g)	E_0 (KJ/mol)	L_0 (nm)	W_0 (cm^3/g)	E_0 (KJ/mol)	L_0 (nm)	S_{mic} (m^2/g)			
AC F400	877	0.350	19.6	1.23	0.259	26.1	0.73	706	0.49	0.54	7.5

Table 3 Prausnitz–Radke adsorption isotherm constants

Adsorbate	a (L/g)	b ($L^{\beta}/mmol^{\beta}$)	B	%D
Phenol	4.37	2.65	0.901	2.1
MB	443.38	667.80	0.816	4.6
MTB	2.75	27.95	0.837	3.9

vary over time, which is why all adsorption rate experiments were carried out at a pH 3 that was constantly maintained. The time to reach equilibrium was 45, 400, and 600 min for phenol, MB, and MTB, respectively, indicating that the overall adsorption rate was associated with the adsorbate molecular size.

The concentration decay curves were carried out at a stirring speed of 400 rpm, because previous experiments showed that external mass transport does not affect the overall adsorption rate at speeds above 400 rpm (See below, Sect. 4.11). The operating conditions for all concentration decay curves are given in Table 4.

4.4 Calculation of mass transport parameters

The experimental value of the molecular diffusivity of phenol in an aqueous solution at infinite dilution was reported to be $D_{AB} = 0.81 \times 10^{-5}$ cm^2/s at 25 °C (Leyva-Ramos and Geankoplis 1994). The Wilke and Chang equation (Poling et al. 2006) was used to estimate the D_{AB} values for MB (5.06×10^{-6} cm^2/s) and MTB (3.15×10^{-6} cm^2/s).

The procedure proposed by Furusawa and Smith (1973) was used to assess the external mass transfer coefficient, based on the fact that when $t \to 0$ then $C_{Ar} \to 0$ and $C_A \to C_{A0}$. Substituting these conditions in Eq. (1), the following equation can be derived:

$$\left[\frac{d\left(\frac{C_A}{C_{A0}}\right)}{dt}\right]_{t=0} = \frac{-mSk_L}{V} \tag{11}$$

The right-hand term in Eq. (11) is the slope of the concentration decay at $t = 0$ and was estimated by using the first two data points of the concentration decay curve ($t = 0$ and 1 min). The k_L values estimated with Eq. (11) are given in Table 4.

4.5 Pore volume diffusion model (PVDM)

The experimental concentration decay curves of phenol, MB, and MTB were interpreted with the PVDM model, which requires determination of D_{ep} and k_L values; k_L was

Table 4 Experimental conditions for the concentration decay curves of phenol, MB, and MTB. T = 298 K, pH 3, V = 0.5 L and 400 rpm

Adsorbate	Run no.	m (g)	C_{A0} (mmol/L)	$C_{e,exp}$ (mmol/L)	q_e (mmol/g)	$k_L \times 10^3$ (cm/s)	$D_{ep} \times 10^7$ (cm^2/s)	$D_s \times 10^8$ (cm^2/s)	%D*
Phenol	1	0.5	1.02	0.34	0.69	7.3	NA	1.38	2.1
	2	0.5	2.04	0.87	1.17	8.1	NA	2.51	3.5
	3	0.5	3.15	1.77	1.38	7.2	NA	2.92	1.1
	4	0.5	4.25	2.66	1.59	10.8	NA	3.40	2.7
	5	0.5	5.30	3.58	1.73	9.8	NA	5.59	4.3
	6	1.0	5.27	2.26	1.51	7.8	NA	4.05	2.2
	7	2.0	5.25	0.79	1.12	5.3	NA	3.40	3.5
MB	8	0.5	0.35	0.01	0.34	10.9	7.99	0.202	1.2
	9	0.5	0.70	0.15	0.55	8.6	7.99	0.232	1.6
	10	0.5	1.06	0.43	0.63	8.8	7.99	0.247	2.1
	11	0.5	1.53	0.81	0.72	7.6	7.99	0.273	5.2
	12	0.5	1.77	1.05	0.72	6.6	7.99	0.303	3.2
	13	1.0	1.74	0.42	0.66	4.2	7.99	0.277	1.1
	14	1.5	1.71	0.07	0.55	2.6	7.99	0.212	0.9
MTB	15	1.0	0.12	0.04	0.039	3.1	5.17	NA	4.8
	16	1.0	0.24	0.13	0.057	2.6	4.45	NA	4.1
	17	1.0	0.37	0.24	0.066	2.3	3.78	NA	4.3
	18	1.0	0.51	0.36	0.073	2.2	3.46	NA	2.5
	19	2.0	0.41	0.16	0.061	1.4	4.72	NA	1.9
	20	3.0	0.39	0.09	0.051	1.7	4.09	NA	3.1

NA not applicable

* Deviation percentage between experimental and predicted curves

estimated using Eq. (11) and D_{ep} was obtained with the following equation:

$$D_{ep} = \frac{D_{AB}\varepsilon_p}{\tau} \tag{12}$$

To apply Eq. (12), it is necessary to know the tortuosity factor of AC F400. Leyva-Ramos and Geankoplis (1994) studied the intraparticle diffusion of several organic compounds on AC F400, finding that τ ranged between 3 and 4.6 and recommending the use of $\tau = 3.5$ for this activated carbon. The D_{ep} values obtained by applying Eq. (12) with $\tau = 3.5$ were 1.28×10^{-6}, 7.99×10^{-7}, and 4.98×10^{-7} cm^2/s for phenol, MB, and MTB, respectively. The concentration decay curves for phenol, MB and MTB (Table 4, runs 5, 12 and 17, correspondingly) are depicted in Fig. 3a–c, as examples, along with the PVDM model predictions. Fig. 3a, b show clearly that the model PVDM does not interpret the experimental data for phenol and MB, substantially overestimating the concentration decay curves. However, Fig. 3c shows that PVDM model fits satisfactorily the experimental data for MTB, indicating its intraparticle diffusion on AC F400 can be controlled by pore volume diffusion.

The numerical solution of the PVDM model was matched with the concentration decay data to find the D_{ep} value best fitted to the experimental data. The optimal value of D_{ep} was evaluated by minimizing the following objective function:

$$\text{Minimum} = \sum_{1}^{N} \left(\phi_{exp} - \phi_{pred}\right)^2 \tag{13}$$

Optimal D_{ep} values were 2.43×10^{-5}, 2.12×10^{-6}, and 3.78×10^{-7} cm^2/s for phenol, MB, and MTB, respectively. These values and the curves predicted with the PVDM model are depicted in Fig. 3, which shows that the PVDM model fitted the experimental data reasonably well. However, the optimal D_{ep} value of phenol was approximately 3-fold higher than the molecular diffusion coefficient of phenol in water, i.e., the phenol molecules diffused much faster within the AC F400 pore volume than in the aqueous solution outside the pores. This result is impossible because D_{ep} must always be lower than the molecular diffusion coefficient. In the case of MB, the optimal D_{ep} value was used to recalculate the value of τ from Eq. (12), giving a value of $\tau = 1.32$, which is very low considering the complex structure of activated carbon given that $\tau = 1$ corresponds to a material with straight pores. These results indicate that the intraparticle diffusion of phenol and MB on AC F400 was not solely due to pore volume diffusion, and another mechanism has to be considered. In contrast, the optimal D_{ep} value for MTB

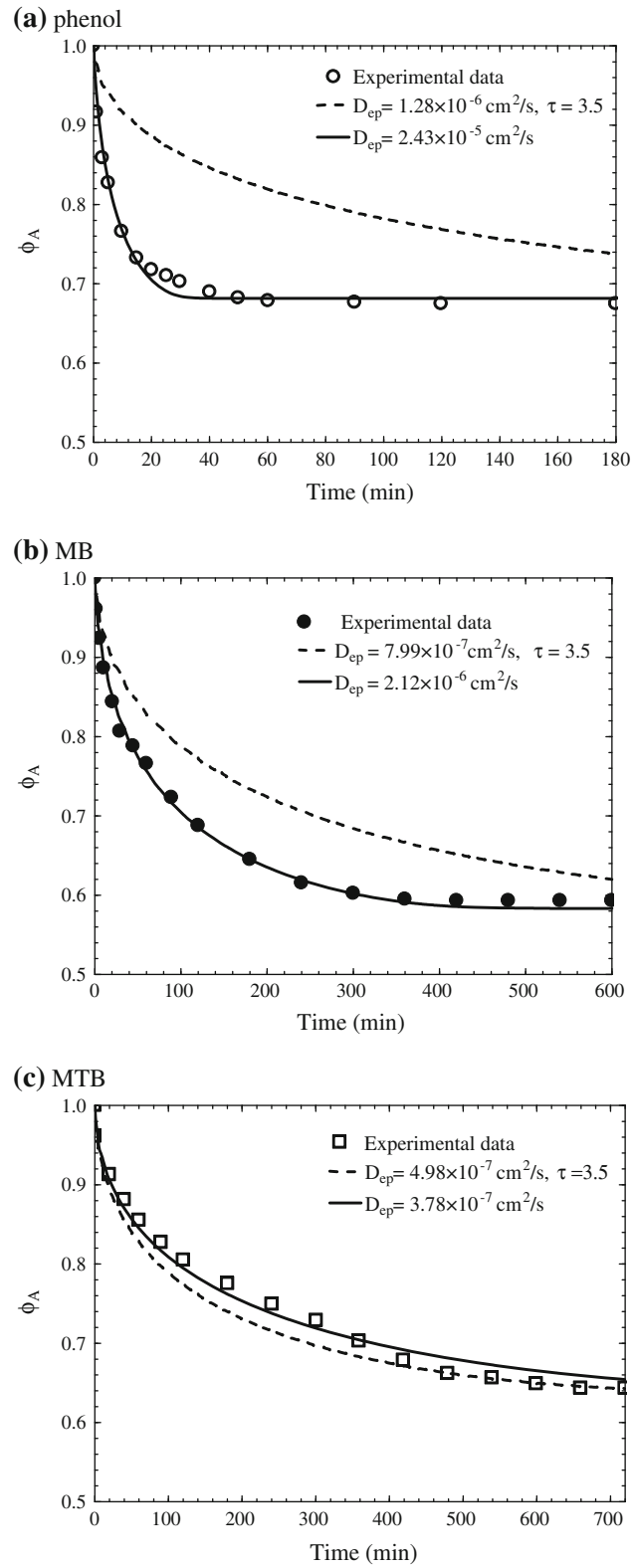

Fig. 3 Concentration decay *curves* for **a** phenol, **b** MB, and **c** MTB adsorption on AC F400 at T = 25 °C. The *lines* represent the PVDM model prediction. Run nos. 5, 12 and 17

was very close to that obtained by applying Eq. (12), which confirms that the intraparticle diffusion mechanism of MTB is controlled by pore volume diffusion.

4.6 Surface diffusional model (SDM)

In the SDM model, the intraparticle diffusion is exclusively due to surface diffusion and, therefore, pore volume diffusion can be ignored. The mass transfer parameters of the SDM model are k_L and D_s, and as described in Sect. 4.4, k_L was estimated with Eq. (11). The value of D_s was assessed by matching the numerical solution of the SDM model with the experimental concentration decay data. The best value of D_s was obtained by minimizing the objective function described by Eq. (13). Figure 4 shows the experimental data for phenol, MB, and MTB (runs 5, 12 and 17) and the prediction of the SDM model with the best value of D_s. It may be observed in this figure that the SDM model satisfactorily fitted the experimental data for phenol, MB and MTB with values of $D_s = 5.59 \times 10^{-8}$, $D_s = 5.30 \times 10^{-9}$ and $D_s = 1.98 \times 10^{-9}$ cm^2/s, respectively. Traegner and Suidan (1989) applied the SDM model to experimental data of *p*-nitrophenol adsorption kinetics on activated carbon AC F400 and obtained a value of $D_s = 1.92 \times 10^{-8}$ cm^2/s, i.e., the same order of magnitude as found in the present study for the phenol molecule. On the other hand, the D_s values obtained for MB and MTB are higher than those found in literature for similar compounds ($D_s = 1.25 \times 10^{-10}$–$4.72 \times 10^{-11}$ cm^2/s) (Choy et al. 2004).

Surface diffusion, i.e., the movement of the adsorbate through the solid surface, is influenced by the distribution of the solid and fluid phases, and the surface concentration gradients are the main driving force. Therefore, in the case of phenol, which has the lowest molecular size and is extendedly adsorbed on AC F400 (Fig. 1), it is expected that its adsorption process was controlled by surface diffusion. For its part, pore volume diffusion refers to the movement of the adsorbate due to concentration gradients in the fluid phase (i.e., molecular mechanisms) and is affected by the geometry of pore. Thus, this model could be appropriate for large size molecules as MB or MTB since they solely diffuse in large pores where the interactions with the pore walls are not strong.

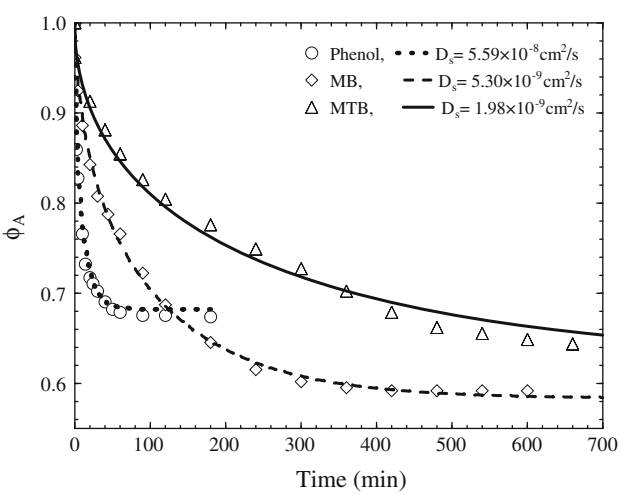

Fig. 4 Concentration decay *curves* for phenol, MB, and MTB adsorption on AC F400 at T = 25 °C. The *lines* represent the SDM model prediction. Run nos. 5, 12 and 17

4.7 Pore volume and surface diffusion model (PVSDM)

The PVSDM model attributes intraparticle diffusion to both pore volume and surface diffusion mechanisms. In order to apply the PVSDM model, k_L was calculated from Eq. (11) and D_{ep} was evaluated with Eq. (12), assuming that $\tau = 3.5$. Hence, the surface diffusion coefficient, D_s, was the only unknown parameter and was evaluated by fitting the numerical solution of the PVSDM model to the concentration decay data. The optimal D_s value was again obtained by minimizing equation (13). Fig. 5a–c depict the experimental concentration decay data for phenol, MB and MTB (runs 5, 12, and 17), respectively and also include the concentration decay curve predicted with the PVSDM model using the optimal D_s values of 6.16×10^{-8}, 4.55×10^{-10} and 3.15×10^{-11} cm^2/s, respectively, showing that this model fitted the experimental data very satisfactorily.

We emphasize that it is common practice to neglect pore volume diffusion when surface diffusion is taking place. However, this assumption has not been substantiated in many published studies on adsorption kinetics in the liquid phase. In order to evaluate the relative contribution of each diffusion mechanism to the overall intraparticle diffusion of adsorbate, the mass transport due to pore volume diffusion, N_{AP}, and the surface diffusion, N_{AS}, were estimated by the following equations:

$$N_{AP} = -D_{ep}\frac{\partial C_{Ar}}{\partial r} \tag{14}$$

$$N_{AS} = -D_s\rho_p\frac{\partial q}{\partial r} \tag{15}$$

The relative contribution of surface diffusion to the overall intraparticle diffusion was estimated with the following equation:

$$\frac{N_{AS}}{N_{AS}+N_{AP}} = \frac{D_s\rho_p\frac{\partial q}{\partial r}}{D_s\rho_p\frac{\partial q}{\partial r}+D_{ep}\frac{\partial C_{Ar}}{\partial r}} \tag{16}$$

The results obtained (not showed) revealed that the contribution of surface diffusion always represented >82 % of the overall intraparticle diffusion in the case of phenol, 5–95 % in the case of MB and 19 % in the case of

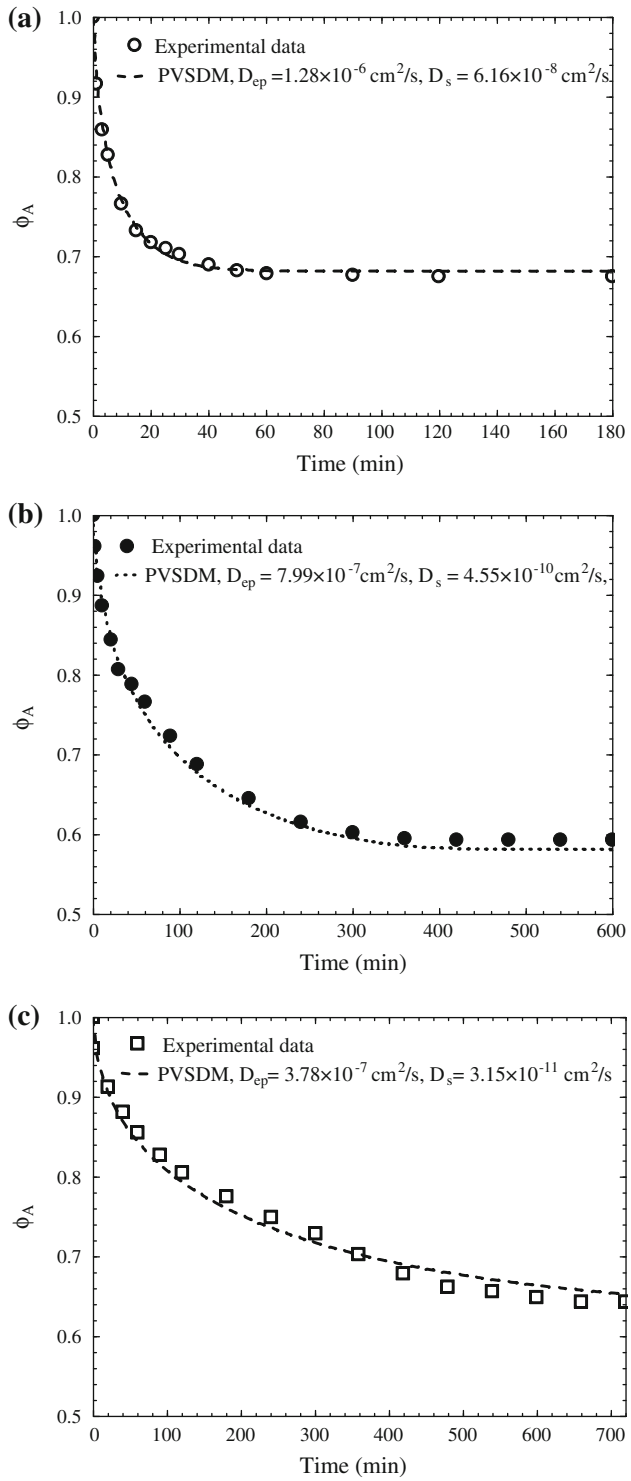

Fig. 5 Concentration decay *curve* for **a** phenol, **b** MB, and **c** MTB adsorption on AC F400. The *lines* represent the PVSDM model prediction. Run nos. 5, 12, and 17

MTB, regardless of the radial position and time. According to these findings, it was corroborated that the intraparticle diffusion during adsorption on AC F400 was due to surface diffusion in the case of phenol, and pore volume diffusion in the case of MTB, while both diffusion mechanisms are important in the case of MB. Based on the above results, the SDM and PVDM models were used in this study to model the experimental data of concentration decay curves for phenol and MTB, respectively, while the PVSDM model was utilized for MB. The results obtained are shown and discussed in the following Sects. 4.7–4.9.

4.8 Interpretation of concentration decay curves of phenol with SDM model

The SDM model was used to interpret the concentration decay curves of phenol at different initial phenol concentrations (runs 1–5, Table 4) and various masses of AC F400 (runs 5–7, Table 4), which yielded different amounts of phenol adsorbed at equilibrium (q_e). The value of D_s was assessed by matching the numerical solution of the SDM model with the experimental concentration decay data. The best D_s value was obtained by minimizing the objective function described by Eq. (13); the results depicted in Fig. 6 and in Table 4 show that the SDM model satisfactorily fitted the experimental data, given that the % D was <4.3 % in all cases and D_s values ranged between 1.38 and 5.59 × 10^{-8} cm^2/s. These D_s values are 10-fold lower than the D_s values found for the adsorption of pyridine on AC F400 (Ocampo-Perez et al. 2010), which may be attributable to the larger molecular size and lower molecular diffusion coefficient of phenol versus pyridine. Traegner and Suidan (1989) applied the SDM model to experimental data of *p*-nitrophenol adsorption kinetics on activated carbon AC F400 and obtained a value of $D_s = 1.92 \times 10^{-8}$ cm^2/s, i.e., the same order of magnitude as found in the present study.

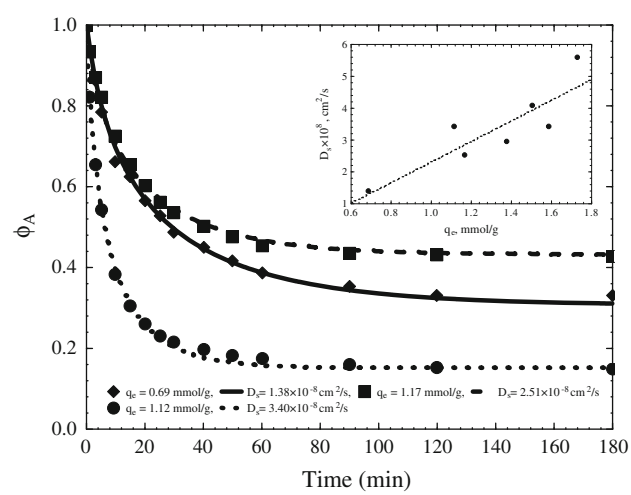

Fig. 6 Concentration decay *curves* for phenol on AC F400 at different mass of phenol adsorbed, q_e. The *lines* represent the SDM model prediction. Run nos. 1, 2 and 7

Data in Fig. 6 also show that D_s values tended to increase with higher q_e. A possible explanation for this trend was that the phenol molecules were initially adsorbed on the most active adsorption sites; therefore, the adsorbed molecules could not be desorbed from a site and diffuse to another. Once the most active adsorption sites were occupied, the phenol molecules would be adsorbed on less active sites, allowing more phenol molecules to be desorbed and move from one site to another, implying an increase in D_s with surface loading. Do (1998), Leyva-Ramos et al. (2009), and Suzuki (1990) reported that surface diffusion was the most important intraparticle diffusion mechanism in adsorbents with a large surface area (activated carbons) and that D_s increased with the mass of solute adsorbed.

4.9 Interpretation of concentration decay curves of MB with PVSDM model

The experimental data for the adsorption rate of MB on AC F400 were interpreted with the PVSDM model (runs 8–14, Table 4) by estimating the D_{ep} value from Eq. (12) and obtaining the optimal D_s value by matching the numerical solution of the PVSDM model with the experimental concentration decay data. The results obtained are given in Table 4 and, as an example, Fig. 7 depicts the concentration decay curves for runs 8, 9 and 14 and the predictions of SDM model. The optimum value of D_s ranged from 2.02×10^{-9} to 3.03×10^{-9} cm^2/s (see Table 4), i.e., an order of magnitude lower than the optimum value for phenol. Al Duri and McKay (1988) studied the adsorption rate of two basic dyes (basic red 22 and basic yellow 21) on AC F400 and reported D_s values of 0.23×10^{-9} and 0.85×10^{-10} cm^2/s, respectively. The adsorption rate of MB on activated carbon prepared from palm kernel shell was satisfactorily interpreted using a film-concentration dependent surface diffusion model, and the D_s values at zero surface coverage ranged from 1.03×10^{-10} to 7.03×10^{-10} cm^2/s (Choong et al. 2006).

Figure 7 also shows that D_s increased with higher q_e, although this increase is considerably lower than that obtained with phenol, largely because a lower amount of MB is adsorbed in comparison to phenol, which decreased the concentration gradients on the surface of activated carbon diminishing the driving force of the surface diffusion (see Fig. 2); therefore, the MB molecules largely occupy higher-energy sites, reducing their mobility.

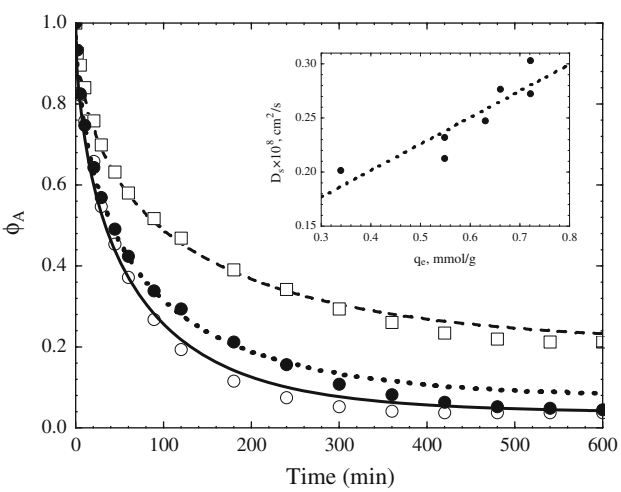

Fig. 7 Concentration decay *curves* for MB on AC F400 at different mass of MB adsorbed, q_e. The *lines* represent the PVSDM model prediction. Run nos. 8, 9 and 14. (*white circles*) $q_e = 0.34$ mmol/g (*dashed lines*) $D_s = 2.02 \times 10^{-9}$ cm^2/s, $D_{ep} = 7.99 \times 10^{-7}$ cm^2/s; (*black circles*) $q_e = 0.55$ mmol/g, (*dashed dotted lines*) $D_s = 2.32 \times 10^{-9}$ cm^2/s, $D_{ep} = 7.99 \times 10^{-7}$ cm^2/s; (*white square*) $q_e = 0.55$ mmol/g, (*dotted lines*) $D_s = 2.12 \times 10^{-9}$ cm^2/s, $D_{ep} = 7.99 \times 10^{-7}$ cm^2/s

4.10 Interpretation of concentration decay curves of MTB with PVDM model

The PVDM model was used to analyze the effect of the mass of MTB adsorbed at equilibrium, q_e, on D_{ep} by varying the initial concentration of MTB and keeping the mass of AC F400 constant and vice versa. The optimum D_{ep} value was again obtained by minimizing the objective function described by Eq. (13). The results presented in Fig. 8 (runs 16, 19 and 20) and in Table 4 (runs 15–20) show that the model fits the experimental data reasonably well (%D <5 %), showing a slight variation in D_{ep} with modifications in the initial MTB concentration and mass of AC F400. Based on the D_{ep} values in Table 4, the τ values were recalculated using Eq. (12) showing a rise in the τ value from 3.4 to 5 with an increase in q_e from 0.039 to 0.073 mmol/g. These results are in agreement with the findings of Leyva-Ramos and Geankoplis (1994) who recommended an τ value of 3.5 for AC F400.

4.11 Effect of external mass transfer on the overall adsorption rate

In a stirred tank adsorber, the external mass transfer is dependent on the agitation speed, particle size and the adsorber geometry. The agitation speed plays a very important role on the operation of a stirred tank adsorber. In this work the speed of the stirrer was fast enough to suspend and mix the activated carbon particles in the adsorber solution, and as low as possible to minimize breaking up the activated carbon particles by attrition.

The effect of external mass transfer on the overall rate of adsorption of phenol, MB and MTB was studied by

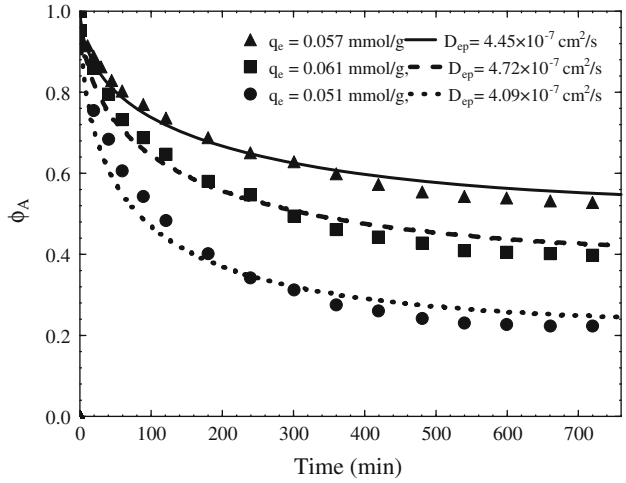

Fig. 8 Concentration decay *curves* for MTB on AC F400 at different mass of MTB adsorbed, q_e. The *lines* represent the PVDM model prediction. Run nos. 1, 2 and 7

performing experiments at the same experimental conditions, but at agitation speeds of 400 and 500 RPM. Figure 9a shows, as an example, the experimental data for the concentration decay curves of phenol at the agitation speeds of 400 and 500 RPM as well as the concentration decay curves predicted with the SDM model. It can be noted that there is no significant difference between the experimental data at both speeds. The external transfer coefficients were estimated to be $k_L = 9.80 \times 10^{-3}$ and $k_L = 9.95 \times 10^{-3}$ cm/s at the agitation speeds of 400 and 500 RPM, respectively (Table 2). These results demonstrated that the effect of the external mass transfer on the overall rate of adsorption can be neglected at agitation speeds above 400 RPM. Similar results were obtained for MB and MTB.

The effect of the activated carbon particle size on the overall adsorption rate was analyzed by carrying out adsorption experiments at the same experimental conditions but using different particle sizes. The average radius were 0.05, 0.010 and 0.005 cm.

As an example, Fig. 9b shows the experimental data for the concentration decay curves of phenol. The values of D_s estimated with the SDM model were 1.38×10^{-8}, 1.33×10^{-8} and 1.25×10^{-8} cm^2/s for the particle radius of 0.050, 0.010 and 0.005 cm, respectively. Hence, D_s did not vary significantly with the particle size of activated carbon. This trend was expected because D_s was affected by the interactions between the phenol molecule and surface of AC F400, but not by the particle size. Besides, the porous structure of the activated carbon was not modified while diminishing its particle size.

The study of the variation of the mass external transport coefficient on the overall adsorption rate of phenol on AC F400 was carried out by comparing the concentration decay curves predicted with SDM model, obtained by

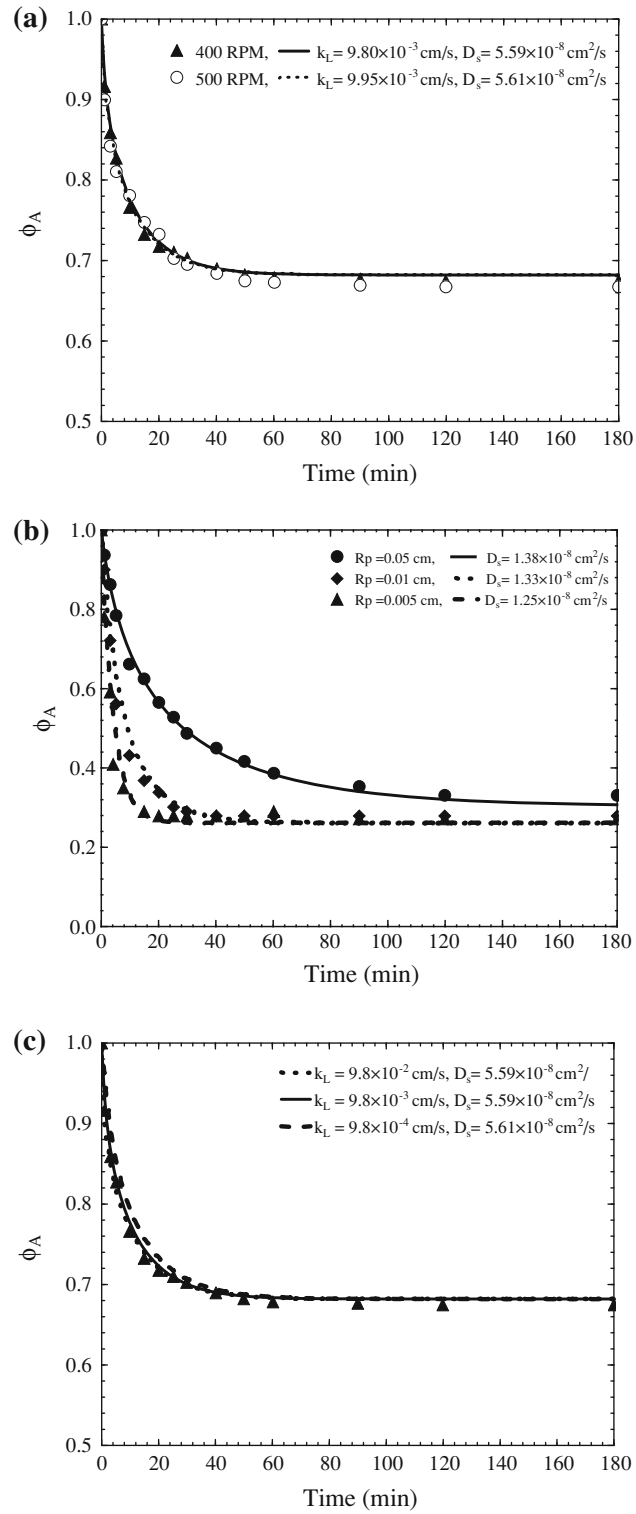

Fig. 9 Effect of **a** agitation speed, **b** particle size and **c** mass external transport coefficient on the concentration decay *curves* for phenol on AC F400

using the optimal value of D_S, for different values of the external mass transfer coefficient, k_L. Thus, the k_L value of 9.8×10^{-3} cm^2/s was increased and diminished 10 times.

Figure 9c depicts the results obtained for Run 5 as an example. The SDM model fitted the experimental adsorption kinetic data independently of the k_L value used. Similar results (not shown) were obtained for MB and MTB adsorption. These results confirm that the adsorption experiments for the three compounds studied were carried out under experimental conditions where the mass external transport did not affect to the overall rate of adsorption.

5 Conclusions

The molecular size of the organic compounds had a major effect on the overall adsorption rate and the controlling mass transfer mechanism. Thus, the diffusional models fitting the experimental adsorption rate data depended on the molecular size of the adsorbate.

The PVSDM model satisfactorily fitted the experimental data, showing that the contribution of surface diffusion always represented >82 % of the overall intraparticle diffusion in the case of phenol, 5–95 % in the case of MB and 19 % in the case of MTB. Accordingly, the controlling mechanism of the overall adsorption rate on AC F400 was surface diffusion for phenol and pore volume diffusion for MTB, while both diffusion mechanisms were important for MB, which is strongly related to their molecular size and adsorption capacity.

The SDM model modeled reasonably well the concentration decay data for phenol adsorption on AC F400 under different experimental conditions. In addition, an increase in D_s was observed with higher q_e.

The PVDM model fitted to the experimental concentration decay data of MTB reasonably well, showing that the tortuosity factor of AC F400 ranged from 3 to 5.

The external mass transport did not affect the overall adsorption rate of phenol, MB and MTB on AC F400.

The realistic values of the diffusion coefficient obtained are: $D_s = 1.38–5.59 \times 10^{-8}$ cm^2/s for phenol, $D_s = 2.02–3.03 \times 10^{-9}$ cm^2/s and $D_{ep} = 7.99 \times 10^{-7}$ cm^2/s for MB and $D_{ep} = 3.46–5.17 \times 10^{-7}$ cm^2/s for MTB.

References

Al Duri, B., Mckay, G.: Basic dye adsorption on carbon using a solid-phase diffusion model. Chem. Eng. J. **38**, 23–31 (1988)

Cañizares, P., Carmona, M., Baraza, O., Delgado, A., Rodrigo, M.A.: Adsorption equilibrium of phenol onto chemically modified activated carbon F400. J. Hazard. Mater. **131**, 243–248 (2006)

Chiang, Y., Chiang, P., Huang, C.: Effects of pore structure and temperature on VOC adsorption on activated carbon. Carbon **39**, 523–534 (2001)

Choong, T.S.Y., Wong, T.N., Chuah, T.G., Idris, A.: Film-pore-concentration-dependent surface diffusion model for the adsorption of dye onto palm kernel shell activated carbon. J. Colloid Interface Sci. **301**, 436–440 (2006)

Choy, K.K.H., Porter, J.F., McKay, G.: Film-surface diffusion during the adsorption of acid dyes onto activated carbon. J. Chem. Technol. Biotechnol. **79**, 1181–1188 (2004)

Diaz-Flores, P.E., Leyva-Ramos, R., Guerrero-Coronado, R.M., Mendoza-Barron, J.: Adsorption of pentachlorophenol from aqueous solution onto activated carbon fiber. Ind. Eng. Chem. Res. **45**, 330–336 (2006)

Do, D.D.: Adsorption Analysis: Equilibria and Kinetics. Imperial College Press, London (1998)

El Qada, E.N., Allen, S.J., Walker, G.M.: Adsorption of basic dyes from aqueous solution onto activated carbons. Chem. Eng. J. **135**, 174–184 (2008)

Fulazzaky, M.A.: Determining the resistance of mass transfer for adsorption of the surfactants onto granular activated carbons from hydrodynamic column. Chem. Eng. J. **166**, 832–840 (2011)

Furusawa, T., Smith, J.M.: Fluid-particle and intraparticle mass transport rates in slurries. Ind. Eng. Chem. Fundam. **12**, 197–203 (1973)

Gil, A., Grange, P.: Application of the Dubinin–Radushkevich and Dubinin–Astakhov equations in the characterization of microporous solids. Colloids Surf. Physicochem. Eng. Asp. **113**, 39–50 (1996)

Karimi-Jashni, A., Narbaitz, R.M.: Impact of pH on the adsorption and desorption kinetics of 2-nitrophenol on activated carbons. Water Res. **31**, 3039–3044 (1997)

Kim, S.J., Kim, S.J., Kim, T.Y., Cho, S.Y.: A study of adsorption behavior of 2,4-Dichlorophenoxyacetic acid onto various GACs. Korean J. Chem. Eng. **19**, 1050–1058 (2002)

Leyva-Ramos, R., Geankoplis, C.J.: Diffusion in liquid-filled pores of activated carbon. I. Pore volume diffusion. Can. J. Chem. Eng. **72**, 262–271 (1994)

Leyva-Ramos, R., Bernal-Jacome, L.A., Mendoza-Barron, J., Hernandez-Orta, M.M.G.: Kinetic modeling of pentachlorophenol adsorption onto granular activated carbon. J. Taiwan Inst. Chem. Eng. **40**, 622–629 (2009)

Mahmudov, R., Huang, C.P.: Selective adsorption of oxyanions on activated carbon exemplified by Filtrasorb 400 (F400). Sep. Purif. Technol. **77**, 294–300 (2011)

Mohan, D., Pittman Jr, C.U., Bricka, M., Smith, F., Yancey, B., Mohammad, J., Steele, P.H., Alexandre-Franco, M.F., Gómez-Serrano, V., Gong, H.: Sorption of arsenic, cadmium, and lead by chars produced from fast pyrolysis of wood and bark during bio-oil production. J. Colloid Interface Sci. **310**, 57–73 (2007)

Ocampo-Perez, R., Leyva-Ramos, R., Alonso-Davila, P., Rivera-Utrilla, J., Sanchez-Polo, M.: Modeling adsorption rate of pyridine onto granular activated carbon. Chem. Eng. J. **165**, 133–141 (2010)

Poling, B.E., Prausnitz, M., O'Connell, J.P.: The Properties of Gases and Liquids. McGraw-Hill, USA (2006)

Rivera-Utrilla, J., Sánchez-Polo, M., Gómez-Serrano, V., Álvarez, P.M., Alvim-Ferraz, M.C.M., Dias, J.M.: Activated carbon modifications to enhance its water treatment applications. An overview. J. Hazard. Mater. **187**, 1–23 (2011)

Sotelo, J.L., Ovejero, G., Delgado, J.A., Martínez, I.: Adsorption of lindane from water onto GAC: Effect of carbon loading on kinetic behavior. Chem. Eng. J. **87**, 111–120 (2002)

Suzuki, M.: Adsorption Engineering. Elsevier, Japan (1990)

Sze, M.F.F., McKay, G.: Enhanced mitigation of para-chlorophenol using stratified activated carbon adsorption columns. Water Res. **46**, 700–710 (2012)

Traegner, U.K., Suidan, M.T.: Parameter evaluation for carbon adsorption. J. Environ. Eng. **115**, 109–128 (1989)

Verma, Y.: Toxicity assessment of dye containing industrial effluents by acute toxicity test using *Daphnia magna*. Toxicol. Ind. Health **27**, 41–49 (2011)

Wibowo, N., Setyadhi, L., Wibowo, D., Setiawan, J., Ismadji, S.: Adsorption of benzene and toluene from aqueous solutions onto activated carbon and its acid and heat treated forms: Influence of surface chemistry on adsorption. J. Hazard. Mater. **146**, 237–242 (2007)

Yang, X., Al-Duri, B.: Kinetic modeling of liquid-phase adsorption of reactive dyes on activated carbon. J. Colloid Interface Sci. **287**, 25–34 (2005)